Structure and mechanical properties of two Mg–Al–Ca alloys consolidated from atomised powder

C. Shaw and H. Jones

Two Mg–Al–Ca alloys (A = Mg–9Al–5Ca; B = Mg–19Al–10Ca, wt-%) have been argon atomised, canned, and then consolidated by extrusion at 280 to 290°C. Alloy B exhibited a compressive fracture strength as high as 720 MPa after 1 h at 300°C while alloy A showed an ultimate tensile strength of 565 MPa and a tensile proof strength of 496 MPa as extruded. The corresponding ultimate strength to density ratios of 400 and 310 MPa m^3 Mg^{-1} of these and other ultrahigh strength rapidly solidified powder metallurgy (RSPM) magnesium alloys exceed or are comparable with the highest available values for ultra high strength RSPM aluminium alloys such as RSPM Al–15Ni–3Mm–5Zr (where Mm is misch metal) and RSPM Al–9·5Zn–3Mg–1·5Cu–4Mn–0·5Zr. *MST/4059*

The authors are in the Department of Engineering Materials, University of Sheffield, Mappin Street, Sheffield S1 3JD, UK.
Manuscript received 20 February 1998; in final form 27 March 1998.

Introduction

The achievement of higher strength in magnesium alloys by combining alloy development with the microstructural refinement or glass formation attainable via rapid solidification processing has been the focus of several research programmes over the past decade.[1–8] Highlights have included tensile yield strengths as high as 480 MPa with an elongation to fracture of 5% in Allied's EA 55RS (Ref. 3) and proof strengths as high as 600 and 740 MPa in Tohoku University's $Mg_{70}Al_{20}Ca_{10}$ (at.-%) and $Mg_{87·5}Y_{7·5}Cu_5$ (at.-%) (Refs. 9, 10). Fracture strengths of melt spun material reached 750 MPa for $Mg_{80}Ni_{10}Ce_{10}$, 800 MPa for $Mg_{85}Cu_5Y_{10}$, 850 MPa for $Mg_{80}Ni_{15}Y_{10}$, and 935 MPa in $Mg_{85}Zn_{12}Ce_3$ (Refs. 2, 5, and 7). Such materials have strength to density ratios as high as 330 MPa m^3 Mg^{-1} which considerably exceed values for the best available high strength aluminium alloys. The present paper is one of a series[11–17] aimed at elucidating strengthening mechanisms in this emerging new class of high strength light alloys and complements an earlier contribution[17] on the structure and properties of melt spun Mg–Al–Ca alloys.

Experimental

Ingots each of mass 3 kg were made by chill casting two Mg–Al–Ca alloys (compositions are given in Table 1) into cast iron moulds of internal diameter 80 mm and height 310 mm. The raw materials for making the alloy were a Domal Mg ingot of 99·99% purity supplied by Magnesium Elektron, an Al ingot of 99·95% purity supplied by Alpoco, and Ca shot of 99·9% purity supplied by Leverton Clarke. Initial melting was carried out in alumina crucibles under vacuum followed by casting under argon. The resulting ingot materials were then remelted at Imperial College for argon updraught atomisation in equipment and using conditions described elsewhere.[18,19] The Coulter method was used for the particle size analysis of the powder produced.

Table 1 Compositions of alloys studied and mean atomised powder particle sizes

Alloy	Al, wt-%	Ca, wt-%	Mg	Max. vol.-% Al_2Ca at equilibrium	Median powder particle size, μm	Mean powder particle size, μm
A	9·1	5·3	Bal.	11	32	79
B	18·8	9·5	Bal.	22	41	79

The resulting particle size distributions are shown in Fig. 1*a* and *b* giving median particle sizes of 32 and 41 μm respectively for alloys A and B. Consolidation was achieved by canning and extrusion at DERA, Farnborough, UK. Powders were packed by tapping to about 60% apparent density in L34 (min. 99·0%Al) containers of internal diameter 38 mm and height 150 mm (Fig. 2).

The can and contents were cold pumped in a vacuum chamber for 16 h to $\sim 6 \times 10^{-6}$ torr ($\sim 8 \times 10^{-6}$ mbar) then heated to 200°C and cooled to 150°C to a final vacuum of $\sim 1 \times 10^{-5}$ torr ($\sim 1·3 \times 10^{-5}$ mbar). Electron beam welding was then employed to seal the can. Extrusion via a 40 mm tapered die was carried out in the temperature range 280–290°C and for an extrusion ratio of 15 : 1. For alloy A breakthrough occurred at an extrusion load of 1·45 MN followed by extrusion at 1·25 MN at a ram speed of 10 mm min^{-1}. For alloy B breakthrough was at 1·55 MN at a ram speed of 0·5 mm min^{-1} which was then increased rapidly to the desired 10 mm min^{-1}. Specimens of the extrudate were characterised both as extruded and after 1 h heat treatment at 100, 200, 300, and 400°C. Specimens from each stage of processing were subjected to optical metallography, X-ray diffraction (XRD) with Co K_α radiation, SEM, and microhardness testing (Knoop or Vickers at a 50 g load). Both alloy powder extrusions were examined by transmission electron microscopy. The inductively coupled plasma method was used for the chemical analysis of the alloys in the as extruded condition (Table 1).

Tensile testing was carried out at room temperature on alloy A extrudate both as extruded and after heat treatment. Specimens conformed to BS EN 10002 with a gauge length of 20 mm and a gauge diameter of 3·99 mm. Mayes testing equipment of capacity 200 kN was used. Extensometer control with a crosshead speed of 0·06 mm min^{-1} was used to obtain a 0·1% proof strength followed by position control with a crosshead speed of 5 mm min^{-1} until failure occurred. Compression tests to failure were carried out at room temperature on both alloys in the as extruded condition and for alloy B after 1 h at 300 and 400°C on the same equipment. Specimens were 3·99 mm in diameter and 6 mm in height. The resulting fracture surfaces from both types of tests were characterised by SEM.

Results

CHILL CAST INGOT AND AS ATOMISED POWDER

The ingot microstructure of alloy A was hypoeutectic with α-Mg dendrites in a eutectic matrix while alloy B was

 ISSN 0267–0836

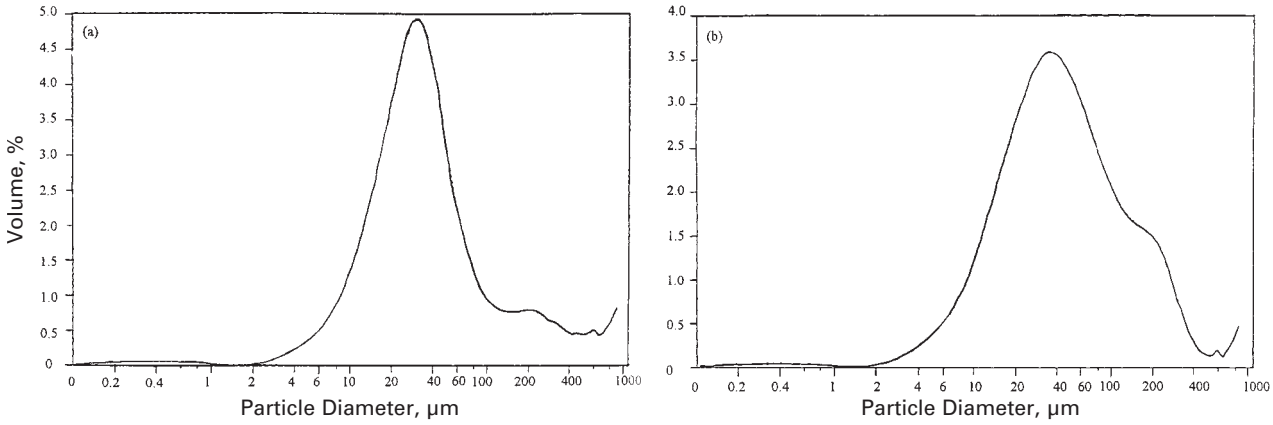

a alloy A; *b* alloy B

1 Volumetric particle size distributions of atomised powder as determined by Coulter laser analysis

hypereutectic with primary Al_2Ca in a matrix of α-Mg dendrites plus eutectic or secondary Al_2Ca (Figs. 3 and 4). The main effect of atomisation was to refine both microstructures by a factor of 10 from a dendrite cell size of ~20 μm as chill cast to ~2 μm, typically, as atomised. The XRD showed all the main α-Mg peaks, the only clear evidence of second phase being from the second strongest Al_2Ca reflection, 222, at $2\theta = 36{\cdot}7^\circ$ for alloy B powder. (The strongest Al_2Ca reflection, 311, at $2\theta = 43{\cdot}3^\circ$ coincides with the strongest α-Mg peak, 101, at $2\theta = 43{\cdot}0^\circ$.) Microhardness measurements gave values of 76 ± 6 and 91 ± 13 kg mm^{-2} for alloy A as chill cast and as atomised respectively, the corresponding values being 96 ± 6 and 105 ± 13 kg mm^{-2} for alloy B.

MICROSTRUCTURE AND MICROHARDNESS OF POWDER EXTRUSIONS

Figure 5 shows optical micrographs of longitudinal sections of the powder extrusions as extruded and after 1 h at 400°C. Banding is evident for both alloys, especially for alloy B. Structure after 1 h at 300°C was not notably different optically from as extruded but in Fig. 5*c* and *d* there are indications of some homogenisation or coarsening after 1 h at 400°C, especially for alloy A. Figure 6 shows transmission electron micrographs of the as extruded condition. Figure 6*a* shows evidence of directionality while more equiaxed structures are shown in Fig. 6*b* and *c*, with alloy B (Fig. 6*c*) being significantly finer in structure than alloy A (Fig. 6*a* and *b*). Microhardness as extruded was

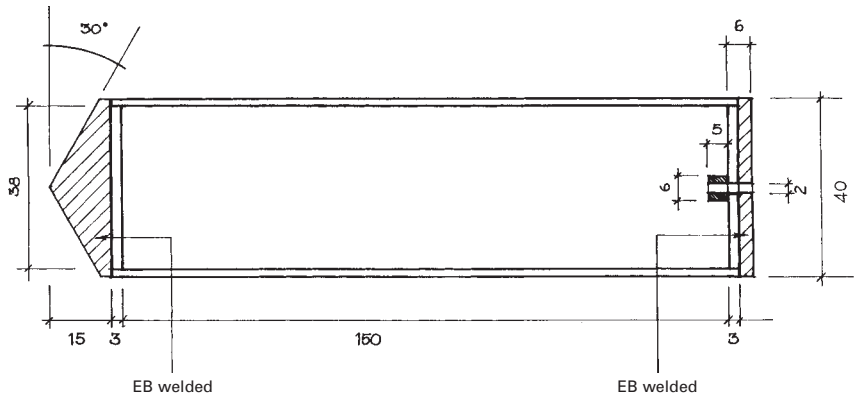

2 Design of can used for powder encapsulation before extrusion: dimensions in millimetres

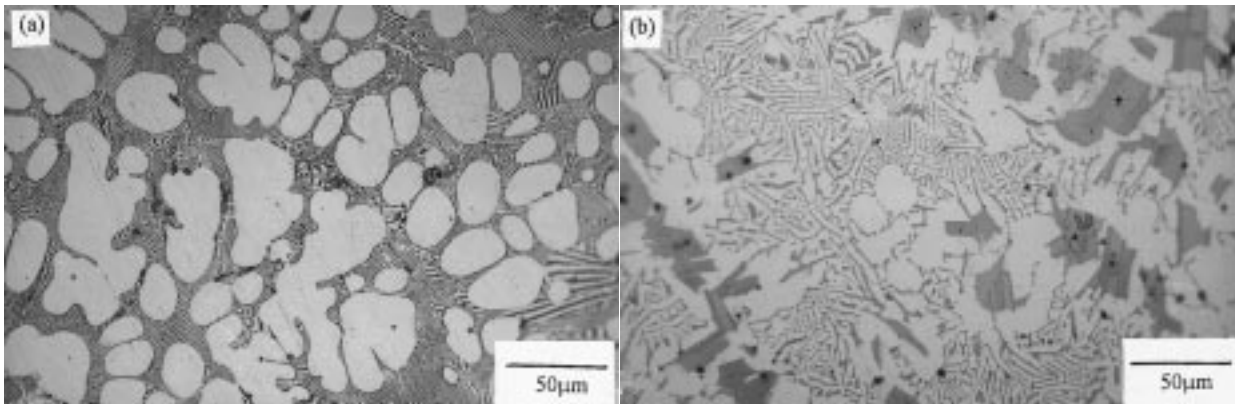

a alloy A; *b* alloy B

3 Microstructures of as chill cast alloys: optical micrographs, as polished

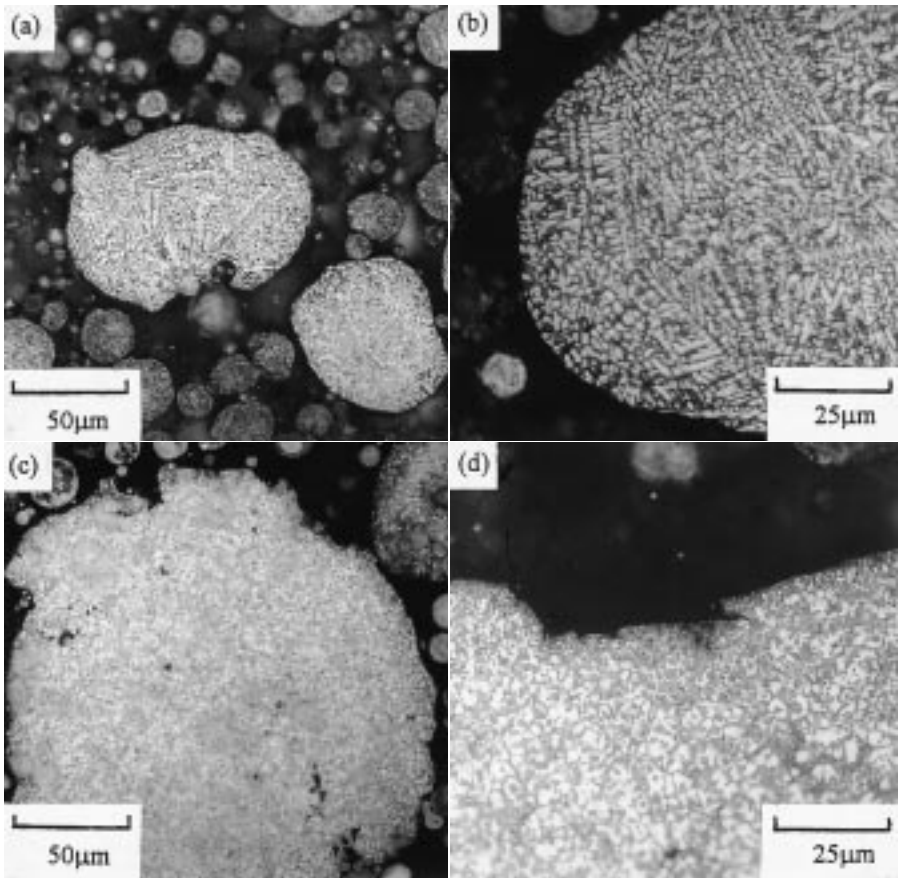

a and *b* alloy A; *c* and *d* alloy B

4 Microstructures of as atomised alloys: optical micrographs, etched for 10 s in 2% nital

$123 \pm 6\ \mathrm{kg\ mm^{-2}}$ for alloy A and $176 \pm 7\ \mathrm{kg\ mm^{-2}}$ for alloy B, these values being retained on isochronal (1 h) heat treatment up to 300°C for alloy A and 200°C for alloy B, and decreasing to 92 ± 3 and $136 \pm 5\ \mathrm{kg\ mm^{-2}}$ respectively after 1 h at 400°C (Table 2).

TENSILE AND COMPRESSIVE TEST DATA

The tensile test results for alloy A powder extrusions are shown in Table 3. They show good reproducibility. After 1 h at 300°C strengths show a reduction of some 20 MPa, but there is a marked improvement in elongation to

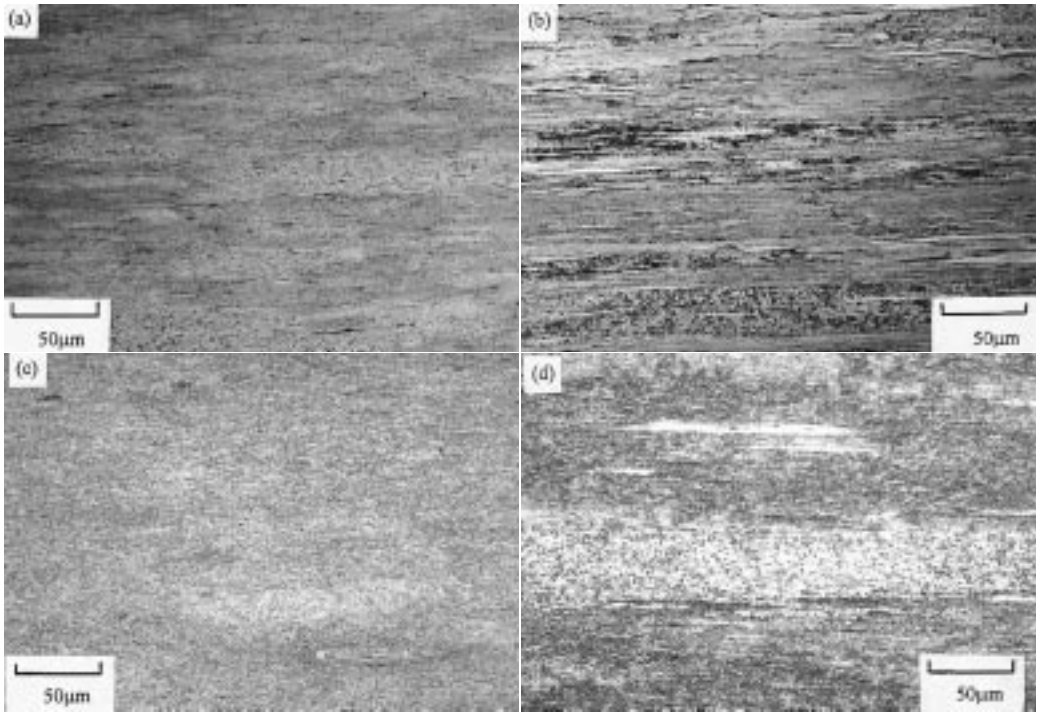

a alloy A, as extruded; *b* alloy B, as extruded; *c* alloy A after 1 h at 400°C; *d* alloy B after 1 h at 400°C

5 Microstructures of extrusions: optical micrographs of longitudinal sections, etched for 10 s in 2% nital

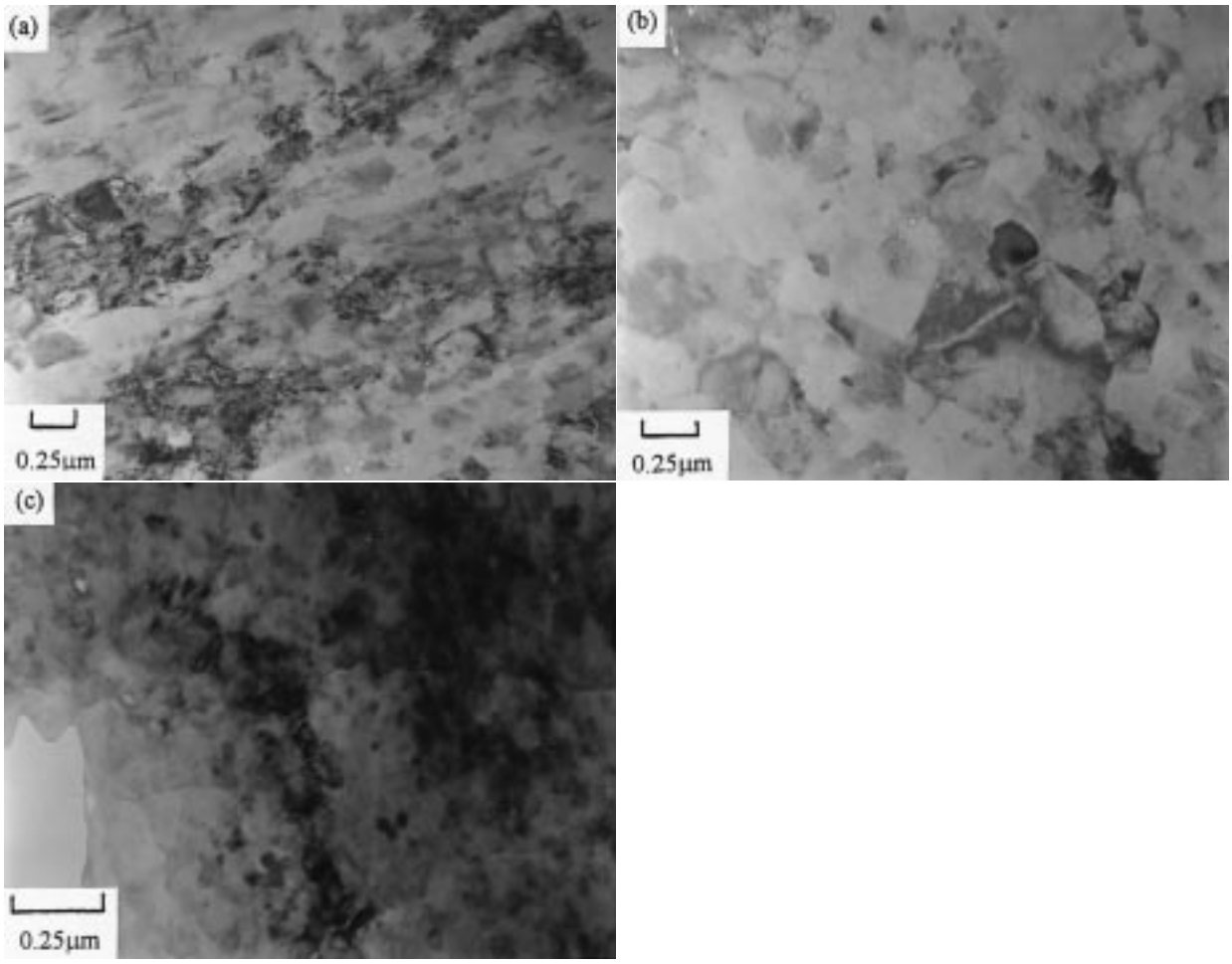

a and *b* alloy A; *c* alloy B

6 Micrographs of alloy powder extrusions as extruded (TEM)

fracture. This improvement was also obtained after 1 h at 400°C but there was a more substantial drop in strength levels. The Young's modulus appeared to increase slightly from $40{\cdot}2 \pm 1{\cdot}5$ GPa as extruded to $43{\cdot}4 \pm 0{\cdot}5$ GPa after 1 h at 300°C and to $44{\cdot}7 \pm 0{\cdot}3$ GPa after 1 h at 400°C. An attempt to test the alloy B powder extrusion in tension was not successful, the specimen failing in a brittle manner at low strain. Figure 7*a* shows part of the fracture surface from the first test for the as extruded condition, in which a crack evidently passes through a prior undeformed powder particle, indicating good cohesion between this particle and the surrounding material.

The results of the compression testing of specimens are given in Table 4. The compressive failure strength of alloy A as extruded (504 ± 32 MPa) was more variable and lower than the tensile fracture strength (561 ± 4 MPa) in Table 3. While the compressive strength of alloy B as extruded was lower than for alloy A, it improved to values as high as

Table 2 Microhardness for the two alloys in various conditions HV(50 g)

Alloy	Ingot, as chill cast	Powder, as atomised	Powder, as extruded	Powder extrusions after 1 h treatment at			
				100°C	200°C	300°C	400°C
A	76 ± 6	91 ± 13	123 ± 6	124 ± 4	123 ± 5	123 ± 5	92 ± 3
B	96 ± 6	105 ± 13	176 ± 7	164 ± 14	171 ± 5	156 ± 7	136 ± 5

Table 3 Tensile test results for alloy A powder extrusions before and after heat treatment

Condition	Test	0·1% proof strength, MPa	Fracture strength, MPa	Elongation to fracture, %	Young's modulus GPa
As extruded	1	496	565	<1	41·7
	3	…	558	<1	40·9
	4	492	560	<1	38·8
1 h at 300°C	5	474	545	4·7	43·9
	6	474	537	2·1	43·0
	7	460	537	1·5	42·9
1 h at 400°C	8	417	461	3·1	45·0
	9	413	459	4·7	44·4
	10	418	462	4·1	44·9

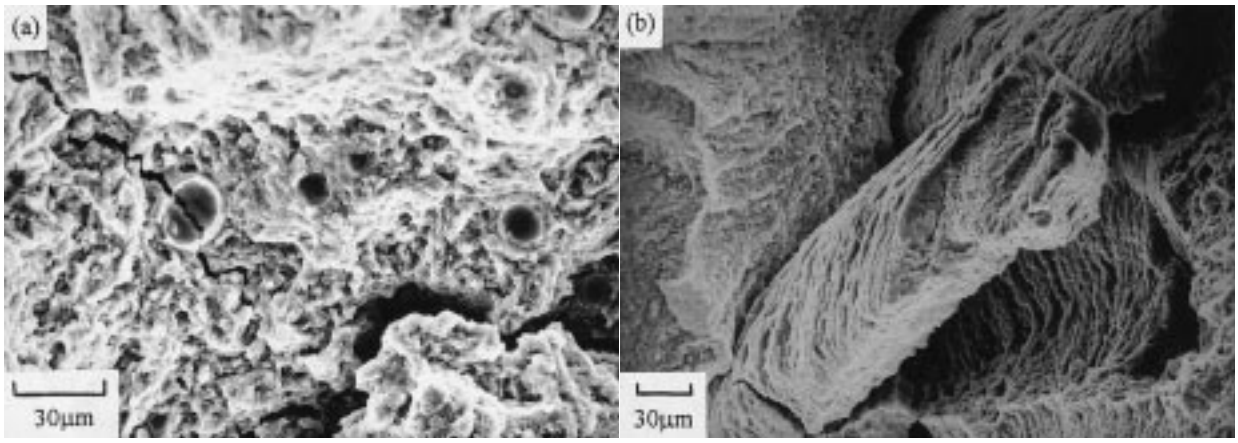

a alloy A as powder extruded (tensile test 1, Table 3) showing a crack passing through a prior powder particle; *b* alloy B powder extrusion after 1 h at 400°C, tested to failure at 574 MPa in compression (Table 4)

7 Secondary electron SEM micrographs of parts of fracture surfaces

720 MPa (606 ± 115 MPa) after 1 h at 300°C and as high as 574 MPa (539 ± 36 MPa) after 1 h at 400°C. Figure 7*b* shows the textured fracture surface of the specimen treated for 1 h at 400°C that failed at 574 MPa and exhibited multiple shear.

Discussion

MICROSTRUCTURE AND HARDNESS AS SOLIDIFIED

The hypoeutectic and hypereutectic microstructures of alloys A (Mg–9Al–6Ca) and B (Mg–18Al–10Ca) as solidified are consistent with previous findings[17] that the eutectic composition of the α-Mg–Al_2Ca pseudobinary lies between 11 and 17 wt-%Al and 8 and 12 wt-%Ca. The refinement in α-Al dendrite cell size λ from ~20 μm as chill cast to 2 μm, typical of the atomised powder, is consistent with an increase in cooling rate $\dot{T}$ during solidification from ~20 to $\sim 2 \times 10^4$ K s^{-1} using the applicable power relationship

$$\lambda = a\,\dot{T}^{-n} \quad . \quad . \quad . \quad . \quad . \quad . \quad . \quad . \quad . \quad . \quad . \quad . \quad . \quad . \quad . \quad (1)$$

with $a = 50$ μm K^n s^{-n} and $n = 1/3$ (Ref. 20). Using the relationship

$$\lambda = b\,d^m \quad . \quad . \quad . \quad . \quad . \quad . \quad . \quad . \quad . \quad . \quad . \quad . \quad . \quad . \quad . \quad (2)$$

where d is droplet particle diameter with $b = 0{\cdot}13$ μm^{1-m} and $m = 2/3$, established experimentally for Ar, N_2, or air atomisation of Al alloy powder,[21] gives

$$\dot{T} = (a/b)^n d^{-mn} = 6 \times 10^7/d^2 \quad . \quad . \quad . \quad . \quad . \quad . \quad . \quad . \quad (3)$$

where $\dot{T}$ is in K s^{-1} and d is in μm; $\dot{T} = 10^4$ K s^{-1} for $d = 80$ μm which is in good accord with the value of 2×10^4 K s^{-1} given directly by the observed λ.

The increase in microhardness of 10 to 20% from the chill cast to the as atomised state in Table 2 is smaller than the increase by factors of up to 2 found for corresponding melt spun Mg–Al–Ca alloys compared with their chill cast state. This larger increase for the melt spun condition is attributable to the formation of an amorphous phase at the higher cooling rates of $\sim 10^6$ K s^{-1} applicable. In the absence of this amorphous phase the size refinement of the α-Mg cell size in the atomised powder would be expected to raise the hardness by some 30 kg mm^{-2}, assuming a Hall–Petch relationship for yield strength σ_y with $k_y = 210$ MPa $\mu m^{1/2}$ (Ref. 11) and that

$$H = 3\sigma_y \quad . \quad . \quad . \quad . \quad . \quad . \quad . \quad . \quad . \quad . \quad . \quad . \quad . \quad . \quad . \quad (4)$$

where H is Vickers hardness (HV 50g). The smaller observed increase suggests that α-Mg dendrite cell boundaries in these microstructures are less effective barriers to propagation of slip or twinning than are the α-Mg grain boundaries to which $k_y = 210$ MPa $\mu m^{1/2}$ is applicable.

Table 4 Compressive fracture strength (MPa) of alloys A and B powder extrusions as extruded and of alloy B after heat treatment (2, 3, or 4 tests per condition)

Alloy	As extruded	After 1 h at 300°C	After 1 h at 400°C
A	473, 515, 536	…	…
B	283, 190	720, 491, 631, 597	574, 503, 540, 538

EFFECT OF EXTRUSION

The banded microstructures in Fig. 5 are typical of atomised powder extrusions. The associated increase in microhardness by about 30 and 70 kg mm^{-2} relative to atomised powder produces a value for alloy B which matches that of mainly amorphous material of similar composition made by melt spinning.[17] The dispersoid sizes of about 0·1 and 0·025 μm evident in the alloy A and B powder extrusions would be expected to give a maximum Orowan contribution to yield stress of magnitude[22]

$$\Delta\sigma = \frac{MYGb(1-0{\cdot}20)^{1/2}}{2\pi(1-\nu^{1/2})} \frac{\ln(3{\cdot}2r/b)}{(L-1{\cdot}6r)} \quad . \quad . \quad . \quad . \quad . \quad . \quad (5)$$

where M is the applicable Taylor factor (6·5 for Mg, Ref. 23), $Y \approx 0{\cdot}9$, G is the shear modulus of the matrix (16·6 GPa, Ref. 24), b is the Burgers vector (0·32 nm, Ref. 24), ν is Poisson's ratio (0·291), L is average centre to centre particle spacing, and r is average dispersoid particle radius. For a random distribution of spherical particles of uniform radius r, we have L given by[25]

$$L = 1{\cdot}23r(2\pi/3f)^{1/2} \quad . \quad . \quad . \quad . \quad . \quad . \quad . \quad . \quad . \quad . \quad . \quad (6)$$

where f is the volume fraction of dispersoid. Using $f = 0{\cdot}11$ and $r = 50$ mm for alloy A and $f = 0{\cdot}22$ and $r = 12{\cdot}5$ nm for alloy B gives $\Delta\sigma = 190$ and 1010 MPa respectively, which are equivalent to microhardness contributions of 60 and 300 kg mm^{-2}, using $\Delta H = 3\Delta\sigma_y$ (Ref. 26). Adding a contribution of 50 kg mm^{-2} from the α-Mg matrix[16] gives a predicted hardness of 110 kg mm^{-2} for alloy A. The prediction for alloy A is similar to the observed value of about 120 kg mm^{-2} but that for alloy B is a factor of 2 too large. This overestimate for alloy B could be at least partly attributable to the non-random distribution of the dispersoid particles, which are not particularly uniform in size. This would reduce the Orowan contribution accordingly.

Table 5 Comparison of strength properties* of high strength (>500 MPa) extruded RSPM magnesium alloys arranged in order of decreasing specific strength

Alloy composition, wt-%	TYS, MPa	UTS, MPa	ε_F, %	E, GPa	ρ, Mg m^{-3}	H, kg mm^{-2}	TYS/ρ, MPa m^3 Mg^{-1}	UTS/ρ, MPa m^3 Mg^{-1}	Ref.
Mg–18Al–10Ca (Alloy B)	...	720†	...	...	1·81	164	...	400†	‡
Mg–20Al–15Ca	600	710	3·4	...	1·81	...	330	390	9
Mg–21Y–10Cu	724	...	...	50	2·21	...	330	...	29
Mg–8Al–5Ga–3Zn	518	646	1·2	48	1·91	168	270	340	8
Mg–9Al–6·5Ca	538	567	3·2	...	1·78	...	300	320	27
Mg–9Al–5Ca (Alloy A)	496	565	...	41	1·78	124	280	320	‡
Mg–9Al–1Zn–1·5Si	468	541	5·4	...	1·82	...	260	300	30
Mg–6Zn–4Ce–0·4Zr	...	554	...	46	1·88	...	...	300	31
Mg–11Si–4Al	455	506	2	...	1·80	...	250	280	32, 33
Mg–5Al–5Zn–5Nd (EA 55RS)	476	513	5·0	46	1·94	...	250	260	3

*TYS tensile yield strength; UTS ultimate tensile strength; ε_F elongation to fracture; E Young's modulus; ρ density; H hardness.
†In compression and after 1 h at 300°C.
‡Present work.

Using the relationship $\sigma_y = H/3$ and the observed H values of 120 and 180 kg mm^{-2} for alloys A and B as extruded predicts flow stresses of 400 and 580 MPa. The predicted 400 MPa for alloy A compares with a measured tensile proof strength of 496 MPa (Table 3). This tensile proof strength is comparable with the 538 MPa reported by Nussbaum *et al.*[27] for pulverised melt spun Mg–9Al–6·5Ca extruded under similar conditions (300°C, 20 : 1, 0·6 m min^{-1}) which also gave a similar ultimate tensile strength (567 MPa). The results of Knoop *et al.*[28] for argon atomised Mg–8·9Al–6·1Ca extruded at 250°C, 25 : 1, and 5–10 mm s^{-1}, however, gave significantly lower strengths (321 and 399 MPa in tension, 468 and 475 MPa in compression). The notably lower and more variable compressive fracture strengths (Table 4) measured for both alloys A and B compared with their values in tension undoubtedly signifies premature fracture initiated by defects which evidently did not occur in the material used by Knoop *et al.* which was in a lower strength condition.

EFFECT OF HEAT TREATMENT

The retention of microhardness of the powder extrusions in 1 h heat treatments up to 300°C (alloy A) and 200°C (alloy B) is in reasonable accord with previous results for melt spun material of similar composition (but mainly amorphous structure).[17] The microhardness of 136 ± 5 kg mm^{-2} for alloy B after 1 h at 400°C, however, exceeds that of the equivalent melt spun material by some 40 kg mm^{-2}. The reduction in microhardness of alloy A by 25% on heat treatment for 1 h at 400°C is larger than the measured reductions by ~17% in tensile proof strength and fracture strength. For alloy B the 12% reduction in average compressive fracture strength from 610 ± 95 MPa after 1 h at 300°C to 540 ± 30 MPa is similar to the corresponding percentage reduction in microhardness from 156 ± 7 to 136 ± 5 kg mm^{-2}. The highest compressive fracture strength of 720 MPa after 1 h at 300°C is similar to that obtained by Kato *et al.*[9] for initially mainly amorphous Mg–Al–Ca alloy powder of similar composition which was devitrified during extrusion at 400°C. Properties of alloys A and B after 1 h at 300°C are compared in Table 5 with results for other extruded high strength (>500 MPa) rapidly solidified powder metallurgy (RSPM) Mg alloys from the literature. Alloy A (Mg–9Al–5Ca) emerges as offering the lowest density together with a strength to density ratio of about 300 MPa m^3 Mg^{-1} while alloy B (Mg–19Al–10Ca) can reach a UTS/ρ of 400 MPa m^3 Mg^{-1} with only a small further increase in density. These values of the strength to density ratio in the upper part of Table 5 already match the highest available values for RSPM Al base alloys, i.e. 320 and 360 MPa m^3 Mg^{-1} for Al–14·9Ni–3·3Mm–5·1Zr (Ref. 34) and 330 MPa m^3 Mg^{-1} for Al–9·5Zn–3·0Mg–1·5Cu–4Mn–0·5Zr (Ref. 35).

Conclusions

1. A compressive fracture strength of 720 MPa has been achieved in a specimen of Mg–19Al–10Ca (wt-%) alloy heat treated for 1 h at 300°C after consolidation of argon atomised powder particulate by extrusion at 290°C.
2. Ultimate tensile strength reached 565 MPa and tensile proof strength reached 496 MPa for the as extruded condition of the more dilute Mg–9Al–5Ca alloy processed in a similar way.
3. Ultimate strength to density ratios of 400 and 310 MPa m^3 Mg^{-1} for these and other ultrahigh strength rapidly solidified powder metallurgy (RSPM) magnesium alloys already exceed or are comparable with the highest available values for RSPM aluminium alloys.

Acknowledgements

This work formed part of a PhD research programme for Miss Shaw at the University of Sheffield funded by an Engineering and Physical Sciences Research Council Case Award with the Defence Research Agency, Fort Halstead.

References

1. S. K. DAS and C. F. CHANG: in 'Rapidly solidified crystalline alloys', 137–156; 1985, Warrendale, PA, TMS.
2. A. INOUE, K. OHTERA, K. KITA, and T. MASUMOTO: *Jpn J. Appl. Phys. 2, Lett.*, 1988, **27**, L2248–L2251.
3. C. F. CHANG, S. K. DAS, D. RAYBOULD, R. L. BYE, and E. V. LIMONCELLI: *Light Met. Age*, 1989, **47**, (9, 10), 12–20.
4. G. NUSSBAUM, P. SAINFORT, G. REGAZZONI, and H. GJESTLUND: *Scr. Metall.* 1989, **23**, 1079–1084.
5. S. G. KIM, A. INOUE, and T. MASUMOTO: *Mater. Trans., JIM*, 1990, **31**, 929–934.
6. A. INOUE, A. KATO, T. ZHANG, S. G. KIM, and T. MASUMOTO: *Mater. Trans., JIM*, 1991, **32**, 609–616.
7. S. G. KIM, A. INOUE, and T. MASUMOTO: *Mater. Trans., JIM*, 1991, **32**, 875–878.
8. T. SHIBATA, M. KAWANISHI, J. NAGAHORA, A. INOUE, and T. MASUMOTO: *Mater. Sci. Eng. A*, 1994, **A179–A180**, 632–636.
9. A. KATO, H. HORIKIRI, A. INOUE, and T. MASUMOTO: *Mater. Sci. Eng. A*, 1994, **A179–A180**, 707–711.

10. T. SUGANUMA, A. KATO, H. HORIKIRI, Y. KAIRAMURA, A. INOUE, and T. MASUMOTO: *Mater. Sci. Eng. A*, 1994, **A179–A180**, 112–117.
11. H. JONES: *Key Eng. Mater.*, 1994, **97–98**, 1–12.
12. Y. LI and H. JONES: *Mater. Sci. Technol.*, 1996, **12**, 651–661.
13. Y. LI and H. JONES: *Mater. Sci. Technol.*, 1996, **12**, 981–989.
14. C. SHAW, Y. LI, and H. JONES: *Mater. Lett.*, 1996, **28**, 33–36.
15. C. SHAW, W. M. RAINFORTH, and H. JONES: *Scr. Mater.*, 1997, **37**, 311–314.
16. C. SHAW and H. JONES: *Mater. Sci. Eng. A*, 1997, **A226–228**, 856–860.
17. C. SHAW and H. JONES: in Proc. 3rd Int. Magnesium Conf., (ed. G. W. Lorimer), Manchester, UK, April 1996, 481–494; 1997, London, Institute of Materials.
18. A. ÜNAL: *Mater. Sci. Technol.*, 1989, **5**, 1027–1033.
19. A. ÜNAL: *Mater. Manuf. Process.*, 1992, **7**, 441–461.
20. C. LABREQUE, R. ANGERS, R. TREMBLAY, and D. DUBE: in 'Light metals', (ed. M. Avedesian and R. Guilbault), 221–231; 1996, Montreal, Canadian Institute of Mining, Metallurgy, and Petroleum.
21. H. JONES: in 'Science and technology of the undercooled melt', (ed. P. R. Sahm *et al.*), 156–185; 1986, Dordrecht, Martinus Nijhoff.
22. E. NEMBACH: 'Particle strengthening of metals and alloys', 242–246; 1997, New York, Wiley.
23. R. ARMSTRONG, I. CODD, R. M. DOUTHWAITE, and N. J. PETCH: *Philos. Mag.*, 1962, **7**, 45.
24. H. J. FROST and M. F. ASHBY: 'Deformation mechanism maps,' 44; 1982, Oxford, Pergamon.
25. M. F. ASHBY: *Z. Metallkd.*, 1964, **55**, 5–17.
26. D. TABOR: 'The hardness of metals'; 1951, Oxford, Oxford University Press.
27. G. NUSSBAUM, G. REGAZZONI, and H. GJESTLUND: in 'Advanced aluminium and magnesium alloys', 789–796; 1990, Materials Park, OH, ASM International.
28. F. M. KNOOP, K. U. KAINER, B. SMOLA, and B. L. MORDIKE: in 'PM '94', Powder Metallurgy World Cong., Vol. 3, 2237–2240; 1994, Les Ulis, Les Editions de Physique.
29. A. KATO, A. INOUE, H. HORIKIRI, and T. MASUMOTO: *Mater. Trans., JIM*, 1995, **36**, 977–981.
30. H. GJESTLUND, G. NUSSBAUM, and G. REGAZZONI: in 'Light weight alloys for aerospace applications', (ed. E. W. Lee *et al.*), 139–149; 1989, Warrendale, PA, TMS.
31. T. SATO, J. KANEKO, and M. SUGAMATA: *J. Jpn Inst. Light Met.*, 1992, **42**, 720–726.
32. M. MABUCHI, K. KUBOTA, and K. HIGASHI: *Scr. Metall. Mater.*, 1995, **33**, 331–335.
33. M. MABUCHI and K. HIGASHI: *Acta Mater.*, 1996, **44**, 4611–4618.
34. H. NAGAHAMA, K. OHTERA, K. HIGASHI, A. INOUE, and T. MASUMOTO: *Philos. Mag. Lett.*, 1993, **67**, 225–230.
35. J. KUSUI, F. FUJII, K. YOKOE, T. YOKOTE, K. OSAMURA, O. KUBOTA, and H. OKUDA: Proc. ICAA5, Grenoble, France, July 1996, *Mater. Sci. Forum*, 1996, **217–222**, 1823–1828.